2022 American Control Conference (ACC)
Atlanta, USA, June 8-10, 2022

# The effect of base flow uncertainty on transitional channel flows

Dhanushki Hewawaduge and Armin Zare

*Abstract*— **We study the effect of white-in-time additive stochastic base flow perturbations on the mean-square properties of the linearized Navier-Stokes equations. Such perturbations enter the linearized dynamics as multiplicative sources of uncertainty. We adopt an input-output approach to analyze the mean-square stability and frequency response of the flow subject to additive and multiplicative uncertainty. For transitional channel flows, we uncover the Reynolds number scaling of critical base flow variances and identify length scales that are most affected by base flow uncertainty. For small-amplitude perturbations, we adopt a perturbation analysis to efficiently compute the variance amplification of velocity fluctuations around the uncertain base state. Our results demonstrate the robust amplification of streamwise elongated flow structures in the presence of base flow uncertainty and that the wall-normal shape of base flow modulations can influence the amplification of various length scales.**

*Index Terms*— **Multiplicative uncertainty, stability analysis, stochastically forced Navier-Stokes, structured uncertainty.**

## I. Introduction

The linearized Navier-Stokes (NS) equations have been shown to capture early stages of transition as well as structural and statistical features of wall-bounded flows. The non-normality of the linearized dynamics induces interactions of exponentially decaying normal modes [1], [2], that result in the high sensitivity of velocity fluctuations to exogenous sources of excitation. This feature has been used to explain the large transient growth of velocity fluctuations [3]–[7] and their amplification due to deterministic and stochastic disturbances in transitional and turbulent wall-bounded flows [8]–[17]. In these studies, additive stochastic excitation is used to model the effect of background exogenous disturbances or the uncertainty caused by excluding nonlinear terms from the linearized equations. A rather less studied aspect arises from the uncertainty surrounding the choice of a base state and its implications for stability analysis.

Typically, linearization happens around a base flow profile that either describes a steady-state solution to the NS equations or a long-time averaged mean of a simulation-based flow field or experimental dataset. This choice depends on the flow configuration and its characteristic regime. The uncertainty caused by insufficient data and imprecise measurements (small-data issues) can often prevail over statistical averaging procedures involved in obtaining the base flow profile. Moreover, the use of modeling approximations/assumptions outside their range of validity and parametric uncertainties can imply a degree of uncertainty in the base state. This motivates an in-depth investigation into the ramifications of base flow uncertainty on the validity and robustness of linear analyses of fluid flows. Prior studies have adopted adjoint-based variational procedures for examining the sensitivity of eigenvalues of the linearized operator [18] or singular values of the frequency response operator [19] to deterministic (worst-case) base flow perturbations. There has also been efforts to quantify the effect of random spatial base flow variations using stochastic spectral projection based on generalized polynomial chaos theory [20].

Additive uncertainty in the base flow enters the linearized dynamics in a multiplicative and structured manner. For deterministic and set-valued uncertainties, the structured singular value can be used to provide a robust stability theory for the uncertain dynamics [21], e.g., this approach was used in [22] to analyze the effect of nonlinearity in transitional channel flows. However, an approach that is based on a worst-case analysis may not provide a realistic model for studying the role experimental/numerical imperfections and measurement noise that are unlikely to bear an optimal shape.

In this paper, we model structured base flow perturbations as white-in-time stochastic processes in the linearized NS equations. While there is no ambiguity in the treatment of additive sources of excitation, the inclusion of multiplicative noise calls for the adoption of a suitable stochastic calculus. Inspired by [23], we provide an appropriate interpretation for the multiplicative uncertainty and reformulate the arising stochastic differential equations (SDEs) as a feedback interconnection of the linearized dynamics and structured stochastic uncertainties thereby separating the nominal dynamics from the sources of uncertainty. We provide specialized conditions for mean-square stability (MSS) and provide a perturbation analysis for studying the energy spectrum of velocity fluctuations in a computationally efficient manner. We use this framework to study the stability and receptivity of channel flow around canonical Couette and Poiseuille profiles that are contaminated with persistent stochastic perturbations as well as the Reynolds number dependence of the energy spectrum of streamwise-constant fluctuations.

The paper is organized as follows. In Sec. II, we present the linearized NS equations around an uncertain base profile and describe our model for base flow perturbations. In Sec. III, we rewrite the linearized dynamics as a feedback interconnection between the nominal dynamics and the sources of uncertainty, provide MSS conditions, and characterize the frequency response. In Sec. IV, we study the stability and receptivity of Couette and Poiseuille flows. In Sec. V, we study the Reynolds number dependence of variance amplification for streamwise elongated flow structures. Finally, we provide concluding remarks in Sec. VI.

Dhanushki Hewawaduge and Armin Zare are with the Department of Mechanical Engineering, University of Texas at Dallas, Richardson, TX 75080, USA. E-mails: {dhanushki.hewawaduge, armin.zare}@utdallas.edu.

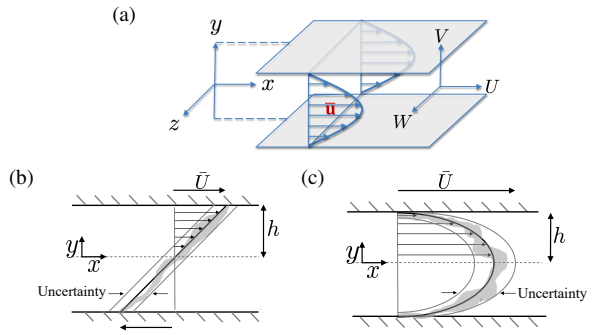


Fig. 1. (a) Pressure driven channel flow with base flow $\mathbf{u} = [1 - y^2 \;\; 0 \;\; 0]$. Side view of three-dimensional Couette (b) and Poiseuille (c) flows along with various realizations of stochastic base flow perturbations $\gamma_u(t)$ represented by the shaded area surrounding the base flow profiles.

## II. Dynamics of Velocity Fluctuations

The hydrodynamic stability of flows is concerned with the behavior of fluctuations around a base state of interest. In plane channel flow (Fig. 1(a)), the dynamics of velocity $\mathbf{v} = [u \;\; v \;\; w]^T$ and pressure $p$ fluctuations around an arbitrary, parallel base flow $\mathbf{u} = [U(y) \;\; 0 \;\; W(y)]^T$ and pressure $P$ are governed by the linearized NS equations,

$$\begin{aligned} \mathbf{v}_t &= -(\nabla \cdot \mathbf{u})\,\mathbf{v} - (\nabla \cdot \mathbf{v})\mathbf{u} - \nabla p + \frac{1}{R}\Delta \mathbf{v} + \mathbf{f} \\ 0 &= \nabla \cdot \mathbf{v} \end{aligned} \tag{1}$$

where $\nabla$ is the gradient, $\Delta = \nabla \cdot \nabla$ is the Laplacian, $t$ is time, and $R = \bar{\mathbf{U}}h/\nu$ is the Reynolds number defined by the maximum nominal velocity $\bar{\mathbf{U}}$, the channel half-height $h$, and the kinematic viscosity $\nu$. In these equations, $\mathbf{f}$ is a three-dimensional zero-mean white-in-time stochastic forcing, which is typically introduced to capture the impact of exogenous excitation sources and initial conditions [11], [16], or to capture the effect of the neglected nonlinearity in the NS equations [14], [15]. We assume the base flow $\mathbf{u}$ to be contaminated with an additive source of uncertainty, i.e., $\mathbf{u}(y,t) = \bar{\mathbf{u}}(y) + \gamma(y,t)$. Here, $\bar{\mathbf{u}} = [\bar{U}(y) \;\; 0 \;\; \bar{W}(y)]^T$ is the nominal base flow and $\gamma$ is a zero-mean white-in-time stochastic process given by $\gamma = [\gamma_u(y,t) \;\; 0 \;\; \gamma_w(y,t)]^T$.

The uncertain base flow $\bar{\mathbf{u}}$ enters the linearized Eqs. (1) as a coefficient that multiplies the vector of velocity fluctuations $\mathbf{v}$. As a result, the evolution of $\mathbf{v}$ is affected by not only the additive source of uncertainty $\mathbf{f}$, but multiplicative sources of uncertainty $\gamma$ that arise form base flow perturbations. While $\mathbf{u}$ includes the sources of uncertainty $\gamma$, it remains constant in $x$ and $z$. Elimination of pressure and application of the Fourier transform in the spatially invariant wall-parallel directions brings Eqs. (1) into the evolution form

$$\begin{aligned} \varphi_t(y,\mathbf{k},t) &= [\mathbf{A}(\mathbf{k},t)\,\varphi(\cdot,\mathbf{k},t)]\,(y) + [\mathbf{B}(\mathbf{k})\,\mathbf{f}(\cdot,\mathbf{k},t)]\,(y) \\ \mathbf{v}(y,\mathbf{k},t) &= [\mathbf{C}(\mathbf{k})\,\varphi(\cdot,\mathbf{k},t)]\,(y) \end{aligned} \tag{2}$$

where the state variable $\varphi = [v \;\; \eta]^T$ contains the wall-normal velocity $v$ and vorticity $\eta = \partial_z u - \partial_x w$, $\mathbf{k} = [k_x \;\; k_z]^T$ is the vector of horizontal wavenumbers over the streamwise and spanwise dimensions, and $v(\pm 1, \mathbf{k}, t) = v_y(\pm 1, \mathbf{k}, t) = \eta(\pm 1, \mathbf{k}, t) = 0$ indicating no-slip/no-penetration boundary conditions on velocity fluctuations.

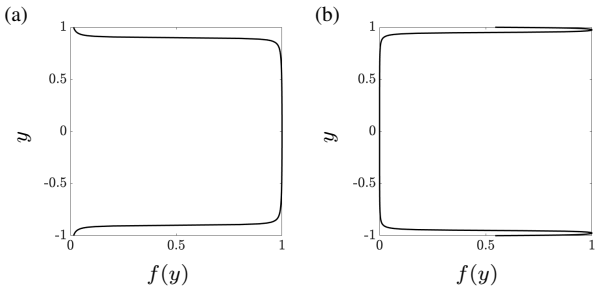


Fig. 2. (a) A shape function $f(y)$ in Eq. (3) with $\{y_1, y_2\} = \{-0.9, 0.9\}$ and $a = 200$; and (b) a two-sided shape function $f(y) = f_1(y) + f_2(y)$ in which $f_1(y)$ and $f_2(y)$ are determined using Eq. (3) with $\{y_1, y_2\} = \{-1, -0.95\}$ for $f_1(y)$, $\{y_1, y_2\} = \{0.95, 1\}$ for $f_2(y)$, and $a = 200$.

Operators $\mathbf{A}$, $\mathbf{B}$, and $\mathbf{C}$ can be found in [24, Eq. (5)].

Herein, we consider the class of stochastic base flow perturbations of the form $\gamma(y,t) = \alpha\,\bar{\gamma}(t) f(y)$, where $\alpha$ is the constant amplitude, $\bar{\gamma}(t)$ is a unit-amplitude zero-mean stochastic parameter of unite amplitude, and

$$f(y) := \frac{1}{\pi}[\arctan(a(y - y_1)) - \arctan(a(y - y_2))] \tag{3}$$

is a smooth filter function that determines the wall-normal region influenced by the stochastic uncertainty. Here, $y_1$ and $y_2$ determine the wall-normal extent of $f(y)$ and $a$ specifies the roll-off rate. We study the influence of stochastic base flow perturbations with wall-normal dependence corresponding to those shown in Fig. 2, as well as a normalized variant of the associated nominal base flow $f(y) = \bar{U}(y)/\max(|\bar{U}(y)|)$.

The operator-valued matrix $\mathbf{A}$ in evolution model (2) can be decomposed into nominal and perturbed components as

$$\mathbf{A}(\mathbf{k},t) = \bar{\mathbf{A}}(\mathbf{k}) + \alpha\,(\bar{\gamma}_u(t)\,\mathbf{A}_u(\mathbf{k}) + \bar{\gamma}_w(t)\,\mathbf{A}_w(\mathbf{k})) \tag{4}$$

where operators $\bar{\mathbf{A}}$, $\mathbf{A}_u$, and $\mathbf{A}_w$ are given in [24, Appendix A]. Here, the nominal base profile $\bar{\mathbf{u}}(y)$, and shape functions $f_u(y)$ and $f_w(y)$ enter operators $\bar{\mathbf{A}}$, $\mathbf{A}_u$, and $\mathbf{A}_w$ as deterministic parameters, respectively.

We discretize operators in (2) in the wall-normal direction using a pseudospectral scheme with $N$ Chebyshev collocation points and follow a change of variables that yields a state-space representation in which the kinetic energy is determined by the Euclidean norm of the state vector [15, Appendix A]. In the resulting state-space model,

$$\begin{aligned} \dot{\boldsymbol{\psi}}(\mathbf{k},t) &= A(\mathbf{k},t)\,\boldsymbol{\psi}(\mathbf{k},t) + B(\mathbf{k})\,\mathbf{f}(\mathbf{k},t) \\ \mathbf{v}(\mathbf{k},t) &= C(\mathbf{k})\,\boldsymbol{\psi}(\mathbf{k},t) \end{aligned} \tag{5}$$

matrices $A$, $B$, and $C$, and state and output vectors $\boldsymbol{\psi} \in \mathbb{C}^{2N}$ and $\mathbf{v} \in \mathbb{C}^{3N}$ represent discretized versions of the corresponding operators in (2).

## III. Mean-Square Stability and Input-Output Analysis

In this section, we adopt an Itō interpretation to treat the sources of multiplicative uncertainty in SDE (5), use a linear fractional transformation to extract these sources of uncertainty from the nominal dynamics, and establish an input-output relation between sources of stochastic excitation and the output velocity fluctuations of system (5).

### A. Stochastic feedback interconnection

In input-output form, SDE (5) can be rewritten as

$$\begin{aligned}\begin{bmatrix}\mathbf{v}(\mathbf{k},t)\\ \mathbf{z}(\mathbf{k},t)\end{bmatrix} &= \int_0^t M(\mathbf{k},t-\tau)\begin{bmatrix}\mathbf{f}(\mathbf{k},\tau)\\ \mathbf{r}(\mathbf{k},\tau)\end{bmatrix}\mathrm{d}\tau\\ \mathbf{r}(\mathbf{k},t) &= \alpha\,\mathcal{D}(\bar{\gamma}(t))\,\mathbf{z}(\mathbf{k},t)\end{aligned} \tag{6}$$

where $\bar{\gamma}$ has been extracted by rearranging the dynamics as a feedback connection between the nominal dynamics and the structured uncertainty $\mathcal{D}(\bar{\gamma}(t)) := \mathrm{diag}\{\bar{\gamma}_u(t)I, \bar{\gamma}_w(t)I\}$, $M$ denotes the finite-dimensional approximation to the impulse response operator $\mathcal{M}$, $\mathbf{v}$ is the output velocity vector (cf. Eqs. (5)), and $\mathbf{z}$ is computed from $\boldsymbol{\psi}$. Moreover, the exogenous stochastic input $\mathbf{f}$, the uncertain feedback signal $\mathbf{r}$, and the sources of uncertainty $\bar{\gamma}_u$ and $\bar{\gamma}_w$ are white processes that are defined as derivatives of Wiener processes [25], i.e.,

$$\bar{\gamma}_i(t) := \frac{\mathrm{d}\tilde{\gamma}_i(t)}{\mathrm{d}t};\;\; \mathbf{f}(\mathbf{k},t) := \frac{\mathrm{d}\tilde{\mathbf{f}}(\mathbf{k},t)}{\mathrm{d}t};\;\; \mathbf{r}(\mathbf{k},t) := \frac{\mathrm{d}\tilde{\mathbf{r}}(\mathbf{k},t)}{\mathrm{d}t}.$$

Here, $\tilde{\gamma}_i(t)$ are zero-mean processes of variance $\sigma_i^2$ with index $i$ denoting $u$ or $w$, $\tilde{\mathbf{f}}(t)$ is a zero-mean process with instantaneous covariance $\left\langle \tilde{\mathbf{f}}(\mathbf{k},t)\,\tilde{\mathbf{f}}^*(\mathbf{k},t)\right\rangle = \Omega(\mathbf{k})\,t$ where $\Omega(\mathbf{k}) = \Omega^*(\mathbf{k}) \succeq 0$ is the spatial covariance matrix. Following [23], we assume that $\tilde{\gamma}_i$ and $\tilde{\mathbf{f}}$ are uncorrelated at all times, adopt the Itō interpretation, and assume that $\mathbf{r}(\mathbf{k},t)$ has temporally independent increments, i.e., its differentials $(\mathrm{d}\mathbf{r}(\mathbf{k},t_1), \mathrm{d}\mathbf{r}(\mathbf{k},t_2))$ are independent when $t_1 \neq t_2$. Based on this, the differential form of Eqs. (6) is given by

$$\begin{aligned}\begin{bmatrix}\mathbf{v}(\mathbf{k},t)\\ \mathbf{z}(\mathbf{k},t)\end{bmatrix} &= \int_0^t M(\mathbf{k},t-\tau)\begin{bmatrix}\mathrm{d}\tilde{\mathbf{f}}(\mathbf{k},\tau)\\ \mathrm{d}\tilde{\mathbf{r}}(\mathbf{k},\tau)\end{bmatrix}\\ \mathrm{d}\tilde{\mathbf{r}}(\mathbf{k},t) &= \alpha\,\mathcal{D}(\mathrm{d}\tilde{\gamma}(t))\,\mathbf{z}(\mathbf{k},t)\end{aligned} \tag{7}$$

and is described by the block diagram in Fig. 3. A corresponding state-space model is given by

$$\begin{aligned}\mathcal{M}:\begin{cases}\mathrm{d}\boldsymbol{\psi}(t) &= \bar{A}\,\boldsymbol{\psi}(t)\mathrm{d}t + B_0\,\mathrm{d}\tilde{\mathbf{r}}(t) + B\,\mathrm{d}\tilde{\mathbf{f}}(t)\\ \mathbf{z}(t) &= C_0\,\boldsymbol{\psi}(t)\\ \mathbf{v}(t) &= C\,\boldsymbol{\psi}(t)\end{cases}\\ \mathrm{d}\tilde{\mathbf{r}}(t) &= \alpha\,\mathcal{D}(\mathrm{d}\tilde{\gamma}(t))\,\mathbf{z}(t).\end{aligned} \tag{8}$$

In these equations, the dependence of vectors and matrices on horizontal wavenumber pair $\mathbf{k}$ is omitted for brevity, and

$$B_0(\mathbf{k}) := \begin{bmatrix} I & I\end{bmatrix},\; C_0(\mathbf{k}) := \begin{bmatrix} A_u(\mathbf{k})^T & A_w(\mathbf{k})^T\end{bmatrix}^T. \tag{9}$$

Here, $\boldsymbol{\psi}$, $\mathbf{z}$, and $\mathbf{v}$ are complex-valued vectors of appropriate dimension, $B$, $C$, $\bar{A}$, $A_u$, and $A_w$ are finite-dimensional approximations of the operators in Eqs. (5) and (4).

### B. Mean-square stability

For the causal LTI system (8), MSS certifies that for all differential inputs, $[\,\mathrm{d}\tilde{\mathbf{f}}\;\; \mathrm{d}\tilde{\mathbf{r}}\,]^T$, with independent increments and uniformly bounded variances, the output process

$$\begin{bmatrix}\mathbf{v}\\ \mathbf{z}\end{bmatrix} = \underbrace{\begin{bmatrix}\mathcal{M}_{11} & \mathcal{M}_{12}\\ \mathcal{M}_{21} & \mathcal{M}_{22}\end{bmatrix}}_{\mathcal{M}}\begin{bmatrix}\mathrm{d}\tilde{\mathbf{f}}\\ \mathrm{d}\tilde{\mathbf{r}}\end{bmatrix}$$

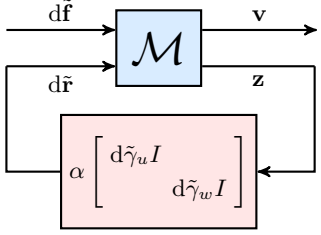


Fig. 3. Linear fractional transformation of an LTI system (8) with $\mathrm{d}\tilde{\mathbf{f}}$ and $\mathrm{d}\tilde{\gamma}_i$ representing differentials of Wiener processes that model additive and multiplicative sources of stochastic uncertainty, respectively.

has a uniformly bounded variance; see, e.g., [26]. Following [27, Theorem 3.2], necessary and sufficient conditions for MSS can be generalized for the continuous-time scenario, i.e., the output $\mathbf{v}$ in (8) has a finite covariance if and only if the feedback subsystem $(\mathcal{M}_{22}, \Gamma)$ is MSS (see, e.g., [27]). Based on this, the exact necessary and sufficient conditions for the MSS of (8) are: (i) $\bar{A}$ is Hurwitz; and (ii) the spectral radius of the loop gain operator

$$\mathbb{L}(\mathbf{R}) := \Gamma \circ \left(\int_0^\infty M_{22}(\tau)\,\mathbf{R}\,M_{22}^*(\tau)\mathrm{d}\tau\right)$$

is strictly less than $1/\alpha^2$, i.e., $\rho(\mathbb{L}) < 1/\alpha^2$. Here, $\circ$ is the Hadamard product, $M_{22}$ is the impulse response of the subsystem $\mathcal{M}_{22} : \mathrm{d}\tilde{\mathbf{r}} \to \mathbf{z}$, which is given by

$$M_{22}(\mathbf{k},t) = C_0(\mathbf{k})\,\mathrm{e}^{\,\bar{A}(\mathbf{k},t)t}\,B_0(\mathbf{k})$$

and $*$ denotes complex-conjugate-transpose. The matrix $\Gamma$ is the mutual correlation of $\tilde{\gamma}_i$, i.e., $\Gamma := \left\langle \tilde{\gamma}_i(t)\,\tilde{\gamma}_j^*(t)\right\rangle$. In this study, we consider $\bar{\gamma}_u$ and $\bar{\gamma}_w$ to be mutually independent, but repeated throughout the spatial domain, i.e., $\Gamma = \mathrm{diag}\{\sigma_u^2\,\mathbb{1}\mathbb{1}^T, \sigma_w^2\,\mathbb{1}\mathbb{1}^T\}$, where $\mathbb{1}$ represents the vector of $2N$ ones. As explained in Sec. II, the wall-normal support of each $\bar{\gamma}_i$ will be captured by its corresponding shape function $f_i(y)$ within operators $A_i$ in Eq. (9).

The loop gain operator propagates the steady-state covariance of $\mathrm{d}\tilde{\mathbf{r}}$ denoted by $\mathbf{R}$ through the feedback configuration in Fig. 3. Equivalently, we have $\mathbb{L}(\mathbf{R}) = \Gamma \circ (C_0\,X\,C_0^*)$, where $X$ is the solution to the algebraic Lyapunov equation

$$\bar{A}\,X + X\,\bar{A}^* = -B_0\,\mathbf{R}\,B_0^*.$$

The spectral radius of $\mathbb{L}$ can be numerically approximated using a power iteration algorithm:

$$\begin{aligned}\bar{A}\,X_{k+1} + X_{k+1}\,\bar{A}^* &= -B_0\,\mathbf{R}_k\,B_0^*\\ \mathbf{R}_{k+1} &:= \frac{1}{\|\mathbf{R}_k\|_F}\left(\Gamma \circ (C_0\,X_{k+1}\,C_0^*)\right)\\ \rho_{k+1} &:= \langle \mathbf{R}_k, \mathbf{R}_{k+1}\rangle.\end{aligned}$$

Here, $\mathbf{R}_0 \succeq 0$ and the algorithm terminates when the residual, $(\mathbf{R}_{k+1} - \rho_{k+1}\mathbf{R}_k)/\|\mathbf{R}_{k+1}\|_F$, is sufficiently small.

### C. Frequency response

The impulse response $M$ in Eq. (7) corresponding to the state-space representation (8) takes the form

$$M(\mathbf{k},t) := \begin{bmatrix}C(\mathbf{k})\\ C_0(\mathbf{k})\end{bmatrix}\mathrm{e}^{\,\bar{A}(\mathbf{k},t)t}\begin{bmatrix}B(\mathbf{k}) & B_0(\mathbf{k})\end{bmatrix}$$

For zero-mean white-in-time processes $\mathbf{f}$, $\bar{\gamma}_u$, and $\bar{\gamma}_w$ with covariance matrix $\Omega$, and variances $\sigma_u^2$ and $\sigma_w^2$, respectively, the steady-state covariance $X(\mathbf{k}) = \lim_{t\to\infty} \langle \boldsymbol{\psi}(\mathbf{k},t)\, \boldsymbol{\psi}^*(\mathbf{k},t)\rangle$ can be obtained by as the solution to the generalized Lyapunov equation

$$\bar{A}\, X + X \bar{A}^* + \alpha^2 B_0 \left(\Gamma \circ (C_0\, X\, C_0^*)\right) B_0^* = -B\, \Omega B^* \quad (10)$$

which is parameterized over $\mathbf{k}$. It can also be used to compute the energy spectrum of velocity fluctuations $\mathbf{v}$,

$$E(\mathbf{k}) \;=\; \mathrm{trace}\left(\Phi(\mathbf{k})\right) \;=\; \mathrm{trace}\left(C(\mathbf{k}) X(\mathbf{k}) C^*(\mathbf{k})\right) \quad (11)$$

where $\Phi(\mathbf{k}) = \lim_{t\to\infty} \langle \mathbf{v}(\mathbf{k},t)\, \mathbf{v}^*(\mathbf{k},t)\rangle$. The influence of multiplicative uncertainty on the energy spectrum can thus be computed as the discounted spectrum

$$E_c(\mathbf{k}) \;=\; E(\mathbf{k}) \;-\; E_0(\mathbf{k}) \quad (12)$$

where $E_0$ denotes the nominal energy spectrum in the absence of multiplicative uncertainties.

Following (9) and the form of $\Gamma$, Eq. (10) can be expanded to reflect contributions from uncertainties that affect the streamwise and spanwise components of the base flow as

$$\bar{A}\, X \;+\; X \bar{A}^* + \\ \alpha^2 \left(\sigma_u^2 (A_u\, X\, A_u^*) + \sigma_w^2 (A_w\, X\, A_w^*)\right) \;=\; -B\, \Omega\, B^* \quad (13)$$

A direct approach to solving (13) as a linear system of equations would involve the use of operator vectorization and matrix inversion. In the absence of sparse matrix structures, this approach can be challenging even for medium-size problems. In what follows, we consider small-amplitude perturbations ($\alpha \ll 1$) and utilize a perturbation analysis to achieve computational efficiency in obtaining the energy spectrum. This approach allows us to compute the second-order statistics of the uncertain model by solving a sequence of standard algebraic Lyapunov equations instead of (13). In addition to the computational benefit, the choice of small perturbations is motivated by the desire to account for uncertainties arising from measurement imperfections, small-data issues in the statistical averaging process, or the effect of active/passive boundary actuation strategies that influence the base flow. Based on this, $X$ is given by the series

$$X(\mathbf{k}) \;=\; X_0(\mathbf{k}) \;+\; \alpha^2\, X_2(\mathbf{k}) \;+\; O(\alpha^4) \quad (14)$$

where $X_0$ and $X_2$ are the state covariance of the nominal dynamics ($\bar{\gamma} = 0$) and its second-order correction induced by random base flow uncertainty, respectively, and are obtained from a set of decoupled Lyapunov equations; see [24, Appendix B] for details. The energy spectrum of velocity fluctuations $\mathbf{v}$ (Eq. (11)) follows a similar perturbation series:

$$E(\mathbf{k}) \;=\; E_0(\mathbf{k}) \;+\; \alpha^2 E_2(\mathbf{k}) \;+\; O(\alpha^4) \quad (15)$$

where $E_0 = \mathrm{trace}(C X_0 C^*)$ is the nominal energy spectrum and $E_2 = \mathrm{trace}(C X_2 C^*)$ captures the effect of base flow perturbations at the level of $\alpha^2$. When $\alpha \ll 1$, the correction $\alpha^2 E_2(\mathbf{k})$ provides a good approximation of the discounted spectrum $E_c(\mathbf{k})$ in Eq. (12), and as $\alpha$ grows, higher-order terms may be needed to approximate $E(\mathbf{k})$.

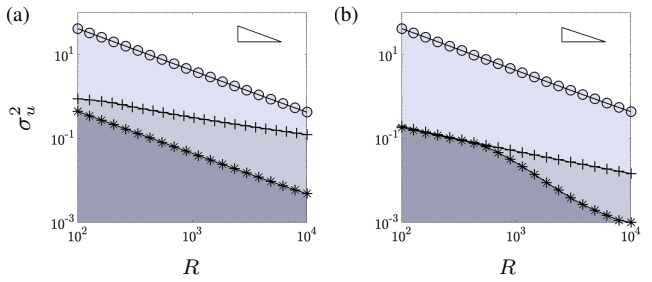


Fig. 4. Stability curves for fluctuations with $\mathbf{k} = (1,1)$ in (a) Couette; and (b) Poiseuille flow demonstrating the Reynolds number dependence of the maximum tolerable variance for base flow perturbations entering the dynamics through $f(y) = \bar{U}(y)/\max(|\bar{U}(y)|)$ (+) or shape functions $f(y)$ in Figs. 2(a) (∗) and 2(b) (○). Shaded areas denote variances of stochastic base flow uncertainty that do not violate MSS ($\rho(\mathbb{L}) < 1$ with $\alpha = 1$). The $R^{-1}$ slope is illustrated by the triangles.

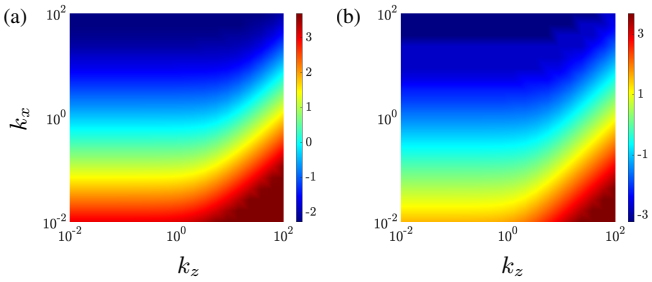


Fig. 5. Logarithmically scaled critical variance levels for stochastic multiplicative uncertainty $\bar{\gamma}_u$ with $\alpha = 1$ and $f(y) = \bar{U}(y)/\max(|\bar{U}(y)|)$ over the horizontal wavenumber spectrum in (a) Couette flow with $R = 500$; and (b) Poiseuille flow with $R = 2000$.

## IV. Base flow variations in transitional flow

We study the effect of zero-mean white-in-time stochastic uncertainty entering the streamwise component of transitional channel flow with $\bar{\mathbf{u}} = [\bar{U}(y)\;\; 0\;\; 0]^T$. For Couette flow $\bar{U}(y) = y$ and for Poiseuille flow $\bar{U}(y) = 1 - y^2$. We use $N = 101$ Chebyshev collocation points to discretize the operators in the linearized equations to examine the MSS of horizontal wavenumber pair $\mathbf{k} = (1,1)$ corresponding to an oblique flow structure. Nonlinear optimal perturbation analysis [28] has demonstrated the fragility of such flow structures in transition mechanisms, i.e., oblique modes require less energy to induce transition than streamwise elongated modes. The MSS conditions provided in the previous section can be used to identify the minimum de-stabilizing variance $\sigma_u^2$. Figure 4 shows the dependence of the critical variance of perturbations on the Reynolds number with the shaded areas under the curves representing asymptotically MSS conditions. Clearly, by confining the wall-normal extent of stochastic perturbations to the vicinity of the walls, larger variances $\sigma_u^2$ can be tolerated. While both flows become less robust to perturbations as the region of influence grows in the wall-normal dimension, the oblique mode in Poiseuille flow is generally more sensitive to channel-wide base flow perturbations ($f(y) = \bar{U}(y)/\max(|\bar{U}(y)|)$ and Fig. 2(a)).

While the flow becomes less stable at higher Reynolds numbers, the critical variance levels show different Reynolds number scaling when the perturbations are bound to different wall-normal regions. In both Couette and Poiseuille flows the critical variance of near-wall base flow pertur-

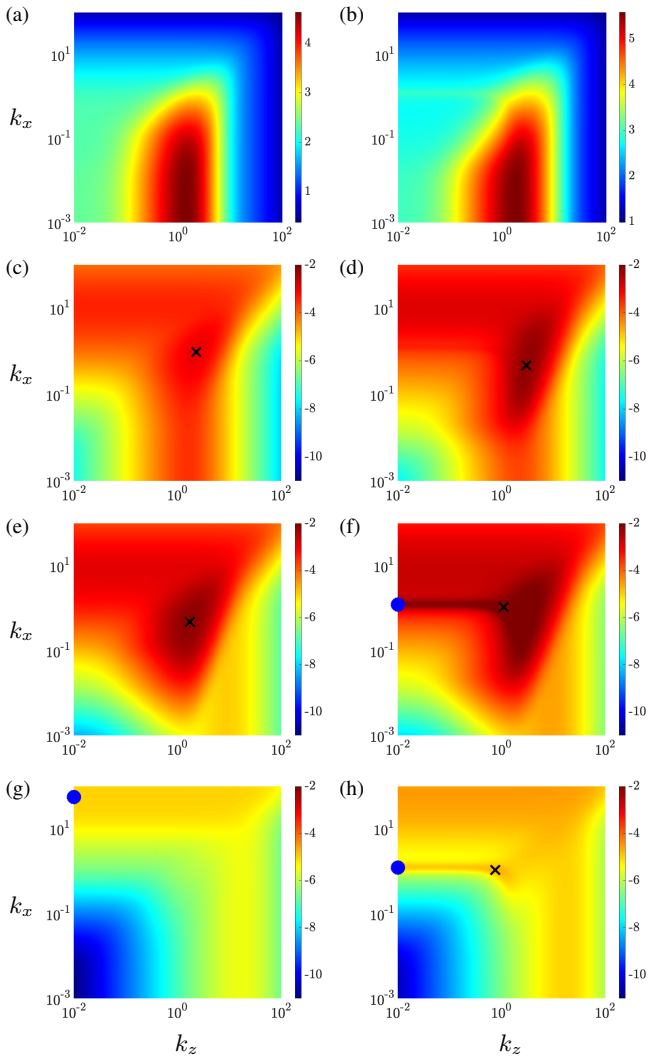


Fig. 6. Nominal energy spectra of (a) Couette flow with $R = 500$ and (b) Poiseuille flow with $R = 2000$ together with corrections $E_2(\mathbf{k})$ due to multiplicative uncertainty $\bar{\gamma}_u$ with $\alpha = 0.01$ (c-h). Shape functions: (c,d) $f(y) = \bar{U}(y)/\max(|\bar{U}(y)|)$; (e,f) Fig. 2(a); (g,h) Fig. 2(b). Variances $\sigma_u^2$: (c) $4.38 \times 10^{-3}$; (d) $6.25 \times 10^{-4}$; (e) 0.004; (f) $6.25 \times 10^{-4}$; (g) 0.005; (h) 0.001. Color plots show $\log_{10}(E_2(\mathbf{k}))$. The symbols ($\times$) and (●) mark wavenumber pairs associated with oblique and TS waves, respectively.

bations (Fig. 2(b)) scale as $R^{-1}$. However, when $f(y) = \bar{U}(y)/\max(|\bar{U}(y)|)$, the critical variance levels decrease at a slower rate ($R^{-1/2}$). Notably, the Reynolds number scaling obtained using our stochastic approach is in agreement with that of [18] for the magnitude of deterministic (worst-case) base flow perturbations. Fig. 5 shows the critical variance levels $\sigma_u^2$ for flow fluctuations with different spanwise and streamwise wavenumbers for $f(y) = \bar{U}(y)/\max(|\bar{U}(y)|)$ in Couette ($R = 500$) and Poiseuille ($R = 2000$) flows. While smaller streamwise wavenumbers corresponding to streamwise elongated structures exhibit more robustness towards base flow perturbations, streamwise elongated structures (streaks) that are thin in the spanwise dimension exhibit the least sensitivity to such base flow uncertainty in both flows.

Using the maximum tolerable variance corresponding to $\mathbf{k} = (100, 0.01)$ in both flows (cf. Fig. 5), we examine the effect of stochastic base flow perturbations on the energy spectrum of velocity fluctuations. For Couette flow with $R = 500$, the critical $\sigma_u^2$ of streamwise base flow perturbations corresponding to $f(y) = \bar{U}(y)/\max(|\bar{U}(y)|)$, Fig. 2(a), and Fig. 2(b) are 0.44, 0.09, and 8.3, respectively. These values change to 0.03, 0.008, and 2.09 for Poiseuille flow with $R = 2000$. The nominal energy spectra $E_0$ of plane Couette and Poiseuille flows computed as the solution of (10) with $\bar{\gamma}_u = 0$ are shown in Fig. 6(a,b). We use perturbation analysis to compute the effect of base flow perturbations on the energy of velocity fluctuations; see [24, Sec. IVB] for a validation study. Figure 6(c-h) shows the second-order correction to the energy spectrum ($E_2(\mathbf{k})$) of channel flow induced by base flow perturbations of various shape $f(y)$. Clearly, base flow perturbations result in the amplification of all spatial scales. While amplification of streamwise elongated flow structures (streaks) dominates the energy spectra of unperturbed flows, small-amplitude channel-wide base flow perturbations (when $f(y) = \bar{U}(y)/\max(|\bar{U}(y)|)$ or Fig. 2(a)) predominantly influence the oblique modes with $k_x \approx 1$ and $k_z \sim O(1)$, and near-wall perturbations (Fig. 2(b)) result in the dominant amplification of 2D Tollmien–Schlichting (TS) waves. As shown in Fig. 6(e,f), streaks are most robust to non-wall-restricted base flow perturbations (Fig. 2(a)), which is in agreement with the worst-case adjoint-based analysis of the zero-pressure-gradient boundary layer [19]. The insensitivity of streaks is because the main diagonal blocks of $A_u$ and $A_w$ are zero for $k_x = 0$; see [24, Appendix A]. Obviously, streaks would become susceptible to such sources of uncertainty if variations were allowed to enter other components of the base state (cf. Figs. 6(c,d) and 6(g,h)).

## V. Reynolds Number Dependence

For any finite $R$, the dynamics of streamwise constant velocity fluctuations ($k_x = 0$) around any parallel base flow subject to streamwise perturbations $\bar{\gamma}_u$ are MSS. Theorem 1 establishes an explicit Reynolds number scaling for the energy spectrum $E(k_z)$ of streamwise constant fluctuations in channel flow subject to streamwise base flow uncertainty.

*Theorem 1:* The variance amplification of streamwise constant velocity fluctuations in channel flow with nominal velocity $\bar{U}(y)$ subject to base flow perturbations is given by

$$E(k_z) \;=\; f(k_z)\,R \;+\; g(k_z)\,R^2 \;+\; h(k_z)\,R^3$$

where the $f$, $g$, and $h$ functions are independent of $R$.

A proof is provided in [24, Appendix D]. Function $f$ does not depend on $\bar{U}(y)$ and is the same for all parallel channel flows. On the other hand, functions $g$ and $h$ depend on the underlying parallel base flow due to their dependence on $\bar{U}'(y)$. In nominal conditions, the energy spectrum of streamwise constant velocity fluctuations of a parallel channel flow can be decomposed into two components that scale with $R$ and $R^3$ [11, Corollary 4]. The effect of base flow uncertainty is exclusively captured by the function $g$, which introduces a $R^2$ scaling to the energy spectrum of velocity fluctuations.

Figure 7 illustrates the $k_z$ dependence of functions $f$, $g$ and $h$ for streamwise constant laminar channel flow subject to both white-in-time exogenous excitation and white-in-time

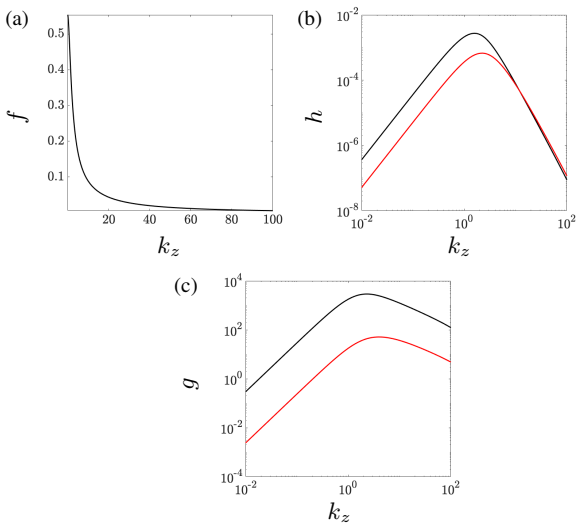


Fig. 7. The $k_z$-dependence of functions $f$, $g$, and $h$ in Theorem 1 for Couette flow with $R = 500$ (—) and Poiseuille flow with $R = 2000$ (—) subject to base flow perturbations of shape $f(y) = \bar{U}(y)/\max(|\bar{U}(y)|)$ and variances $\sigma_u^2 = 1.13 \times 10^5$ and $\sigma_u^2 = 3223$, respectively.

base flow perturbations with $f(y) = \bar{U}(y)/\max(|\bar{U}(y)|)$. The function $h$, which corresponds to the dominant Reynolds number scaling ($O(R^3)$) at high Reynolds numbers, peaks at around the same spanwise wavenumber ($k_z = 1.59, 2.09$ in Couette and Poiseuille flows, respectively) as the nominal energy spectra peak (cf. Figs. 6(a) and 6(b)). Figure 7(c) shows the $k_z$ dependence of the function $g$, which scales as $R^2$, in the presence of streamwise base flow perturbations $\bar{\gamma}_u$ with $\alpha = 1$. The spanwise wavenumbers at which the function $g$ peaks for these two flows ($k_z = 1.91, 3.02$, in Couette and Poiseuille flows, respectively) is in agreement with the energy spectra in Figs. 6(c) and 6(d) for $k_x \approx 0$.

## VI. Concluding Remarks

In this study, we provide an input output analysis to study the stability and frequency response of velocity fluctuations in channel flow subject to stochastic perturbations in the base profile. We provide verifiable conditions for the MSS of the linearized dynamics around the uncertain base flow and obtain the second-order statistics of flow by solving a set of generalized Lyapunov equations. As case studies, we consider the plane Couette and Poiseuille flows subject to white-in-time base flow variations entering at different wall-normal regions. We show that the Reynolds number dependence of critical destabilizing uncertainty variances uncovered by our method are in agreement with previously reported scaling laws for the magnitude of deterministic base flow variations. Furthermore, for small-amplitude base flow perturbations, we adopt a perturbation analysis to compute the energy spectrum of velocity fluctuations using a computationally efficient method that bypasses the need to solve generalized Lyapunov equations. Our results demonstrate the robust amplification of streamwise elongated flow structures as well as the dominant amplification of oblique modes and TS waves in the presence of base flow perturbations of different wall-normal shape and variance levels. Finally, we study the Reynolds number dependence of the energy spectrum (square of $\mathcal{H}_2$ norm) of streamwise constant fluctuations and uncover an additional scaling term relative to the nominal case that scales as $R^2$.

## References


[1] L. N. Trefethen, A. E. Trefethen, S. C. Reddy, and T. A. Driscoll, "Hydrodynamic stability without eigenvalues," *Science*, vol. 261, pp. 578–584, 1993.

[2] P. J. Schmid and D. S. Henningson, *Stability and Transition in Shear Flows*. New York: Springer-Verlag, 2001.

[3] L. H. Gustavsson, "Energy growth of three-dimensional disturbances in plane Poiseuille flow," *J. Fluid Mech.*, vol. 98, p. 149, 1991.

[4] K. M. Butler and B. F. Farrell, "Three-dimensional optimal perturbations in viscous shear flow," *Phys. Fluids A*, vol. 4, p. 1637, 1992.

[5] S. C. Reddy and D. S. Henningson, "Energy growth in viscous channel flows," *J. Fluid Mech.*, vol. 252, pp. 209–238, 1993.

[6] D. S. Henningson and S. C. Reddy, "On the role of linear mechanisms in transition to turbulence," *Phys. Fluids*, vol. 6, no. 3, pp. 1396–1398, 1994.

[7] P. J. Schmid and D. S. Henningson, "Optimal energy density growth in Hagen-Poiseuille flow," *J. Fluid Mech.*, vol. 277, pp. 197–225, 1994.

[8] B. F. Farrell and P. J. Ioannou, "Perturbation growth in shear flow exhibits universality," *Phys. Fluids A*, vol. 5, no. 9, pp. 2298–2300, 1993.

[9] B. F. Farrell and P. J. Ioannou, "Perturbation structure and spectra in turbulent channel flow," *Theoret. Comput. Fluid Dynamics*, vol. 11, pp. 237–250, 1998.

[10] B. Bamieh and M. Dahleh, "Energy amplification in channel flows with stochastic excitation," *Phys. Fluids*, vol. 13, no. 11, pp. 3258–3269, 2001.

[11] M. R. Jovanovic and B. Bamieh, "Componentwise energy amplification in channel flows," *J. Fluid Mech.*, vol. 534, pp. 145–183, July 2005.

[12] Y. Hwang and C. Cossu, "Amplification of coherent streaks in the turbulent Couette flow: an input-output analysis at low Reynolds number," *J. Fluid Mech.*, vol. 643, pp. 333–348, 2010.

[13] Y. Hwang and C. Cossu, "Linear non-normal energy amplification of harmonic and stochastic forcing in the turbulent channel flow," *J. Fluid Mech.*, vol. 664, pp. 51–73, 2010.

[14] B. J. McKeon and A. S. Sharma, "A critical-layer framework for turbulent pipe flow," *J. Fluid Mech.*, vol. 658, pp. 336–382, 2010.

[15] A. Zare, M. R. Jovanovic, and T. T. Georgiou, "Colour of turbulence," *J. Fluid Mech.*, vol. 812, pp. 636–680, February 2017.

[16] W. Ran, A. Zare, M. J. P. Hack, and M. R. Jovanovic, "Stochastic receptivity analysis of boundary layer flow," *Phys. Rev. Fluids*, vol. 4, no. 9, p. 093901 (28 pages), September 2019.

[17] A. Zare, T. T. Georgiou, and M. R. Jovanovic, "Stochastic dynamical modeling of turbulent flows," *Annu. Rev. Control Robot. Auton. Syst.*, vol. 3, pp. 195–219, May 2020.

[18] A. Bottaro, P. Corbett, and P. Luchini, "The effect of base flow variation on flow stability," *J. Fluid Mech.*, vol. 476, pp. 293–302, 2003.

[19] L. Brandt, D. Sipp, J. O. Pralits, and O. Marquet, "Effect of base-flow variation in noise amplifiers: the flat-plate boundary layer," *J. Fluid Mech.*, vol. 687, pp. 503–528, 2011.

[20] J. Ko, D. Lucor, and P. Sagaut, "Effects of base flow uncertainty on Couette flow stability," *Comput. Fluids*, vol. 43, no. 1, pp. 82–89, 2011.

[21] S. Skogestad and I. Postlethwaite, *Multivariable feedback control: analysis and design*. Wiley New York, 2007, vol. 2.

[22] C. Liu and D. F. Gayme, "Structured input-output analysis of transitional wall-bounded flows," *J. Fluid Mech.*, vol. 927, 2021.

[23] M. Filo and B. Bamieh, "An input-output approach to structured stochastic uncertainty in continuous time," *arXiv preprint arXiv:1806.09091*, 2018.

[24] D. B. Hewawaduge and A. Zare, "Input-output analysis of stochastic base flow uncertainty," *Phys. Rev. Fluids*, 2021.

[25] B. Øksendal, "Stochastic differential equations," in *Stochastic differential equations*. Springer, 2003, pp. 65–84.

[26] J. Samuels, "On the mean square stability of random linear systems," *IRE Trans. Circuit Theory*, vol. 6, no. 5, pp. 248–259, 1959.

[27] M. Filo and B. Bamieh, "An input-output approach to structured stochastic uncertainty," *IEEE Trans. Automat. Control*, 2020.

[28] S. M. E. Rabin, C. P. Caulfield, and R. R. Kerswell, "Triggering turbulence efficiently in plane Couette flow," *J. Fluid Mech.*, vol. 712, p. 244, 2012.